Reprogramming the posttranslational code of SRC-3 confers a switch in mammalian systems biology

Brian York[a], Chundong Yu[a,b], Jørn V. Sagen[a,c,d], Zhaoliang Liu[a,e], Bryan C. Nikolai[a], Ray-Chang Wu[a], Milton Finegold[f], Jianming Xu[a], and Bert W. O'Malley[a,1]

[a]Department of Molecular and Cellular Biology, Baylor College of Medicine, Houston, TX 77030; [b]Key Laboratory of the Ministry of Education for Cell Biology and Tumor Cell Engineering, School of Life Sciences, Xiamen University, Xiamen, Fujian 361005, China; [c]Institute of Medicine, University of Bergen, N-5021 Bergen, Norway; [d]The Hormone Laboratory, Haukeland University Hospital, N-5021 Bergen, Norway; [e]Institute of Biosciences and Technology, Texas A & M Health Science Center, Houston, TX 77030; and [f]Department of Pathology, Baylor College of Medicine, Houston, TX 77030

Contributed by Bert W. O'Malley, April 29, 2010 (sent for review December 21, 2009)

Here we demonstrate that reprogramming steroid receptor coactivator-3 (SRC-3) function by changing its posttranslational modification (PTM) code drastically influences systems biology. These findings support the physiological importance of PTMs in directing in vivo functions of a master coregulator. We previously reported that the transactivation potential of SRC-3 is controlled in part by PTMs, although this data emanated from in vitro studies. To test the physiological implications of PTMs on SRC-3, we developed a knock-in mouse model containing mutations at four conserved phosphorylation sites. These mice displayed a systems biology phenotype with increased body weight and adiposity, coupled with reduced peripheral insulin sensitivity. Collectively, these phenotypes result from increased IGF1 signaling, due to elevated IGFBP3 levels. We provide convincing evidence that these mutations in SRC-3 promoted enhanced transcription of the IGFBP3 gene and globally influenced growth and metabolism. Consequently, these mice displayed increased liver tumorigenesis, which likely results from elevated IGF1 signaling.

coactivator | metabolism | posttranslational modification | obesity

Gene expression is a highly coordinated process that requires a delicate crosstalk between the basal transcriptional machinery, transcription factors, and transcriptional coregulators. Built into each of these components is an evolutionarily tuned code of posttranslational modifications (PTMs) that regulate the activity, association/dissociation, localization, and turnover of many proteins. This regulation is especially true for the p160 family of coactivators, whose global function, enzymatic activity, and stability are tightly controlled by PTMs (1–4).

The p160 family of coactivators, which include steroid receptor coactivator (SRC)-1, SRC-2, and SRC-3 (AIB1, p/CIP, NCoA3) have pleiotropic effects in different physiological systems (5). Central to these physiological functions are the unique roles these coactivators play in maintenance of metabolic homeostasis. Although these three coactivators are critical for preserving normal metabolic function, each coactivator has a selective role in energy homeostasis. For example, SRC-1 plays a key role in regulation of energy expenditure, and its deletion confers susceptibility to diet-induced obesity (6). Additionally, SRC-1 seems to be an important regulator of hepatic gluconeogenesis and coordinates regulation of protein metabolism. By contrast, deletion of SRC-2 provides protection against diet-induced obesity through enhanced energy expenditure (6). Moreover, we have shown that SRC-2 is important for hepatic glucose output (7). Lastly, ablation of SRC-3, which is essential for maintenance of white adipose tissue differentiation, protects against obesity and improves insulin sensitivity (8, 9). Collectively, these findings establish the p160 family of coactivators as important regulators of metabolic homeostasis.

In line with its metabolic functions, SRC-3 has been shown to dynamically regulate cell proliferation (10). Amplification of SRC-3 has been reported in numerous cancers such as breast, prostate, lung, colorectal, pancreatic, and liver (5). Mechanistically, SRC-3 exerts its influence on cell growth by serving as an integrator of multiple proliferative pathways. SRC-3 interacts with, and stimulates the transcriptional output of powerful oncogenes such as E2F1, HER2/*neu*, C/EPBβ, and NFκB, each of which regulates distinct components of the proliferative machinery (8, 11–13). In addition to these growth regulators, SRC-3 expression and activity are closely and positively associated with the IGF1 signaling pathway. Loss of the SRC-3 gene confers a reduction in circulating IGF1, primarily due to a decrease of IGFBP3 levels (14). Consequently, multiple downstream pathways of AKT signaling are affected, leading to a deficiency in growth-related targets such as cyclin D1 and β-catenin (15, 16). Much of SRC-3 function in proliferation is thought to be facilitated through changes in the posttranslational code of the protein. We have found that the SRC-3 coactivator contains >50 authentic PTMs of various types. Work in cultured cells from our laboratory clearly established that site-specific phosphorylation events not only impact SRC-3′s transcriptional activity and transcription factor selectivity, but also facilitate turnover of activated SRC-3 upon completion of transcription (3). Numerous in vitro and in vivo studies have established SRC-3 as a key regulator of systems biology (17). Moreover, cell-based and cell-free systems have clearly demonstrated a mechanistic role for PTMs in controlling SRC-3 function and activity. In the present study, we developed a knock-in mouse model containing mutations in four conserved phosphorylation sites in SRC-3. Interestingly, the effects of these mutations result in phenotypes opposite to the SRC-$3^{-/-}$ mouse model, including increased body weight and adiposity, decreased metabolic rate, and the development of insulin resistance. Collectively, our results provide evidence that changes in the functional PTM code of a nuclear receptor coactivator (SRC-3) confer systemic changes in growth and metabolism in the absence of an alteration in the normal levels of the protein.

Results

Generation of SRC-$3^{\Delta/\Delta}$ Knock-in Mice. To evaluate the in vivo function of PTMs in SRC-3, we generated a knock-in mouse model harboring alanine mutations in four phosphorylation sites conserved in human and mouse SRC-3 (Fig. 1*A*, Fig. S1A, and Table S1). As confirmed by Southern blot, the targeted homologous recombination in ES cells resulted in the successful insertion of the mutations and the selection marker (Fig. S1*B*). Positively identified clones validated by DNA sequencing to confirm the

Author contributions: B.Y., C.Y., and B.W.O. designed research; B.Y., C.Y., J.V.S., Z.L., and B.N. performed research; B.Y., R.-C.W., M.F., and J.X. contributed new reagents/analytic tools; B.Y., C.Y., J.V.S., Z.L., B.N., M.F., and J.X. analyzed data; and B.Y. wrote the paper.

The authors declare no conflict of interest.

Freely available online through the PNAS open access option.

[1]To whom correspondence should be addressed. E-mail: berto@bcm.tmc.edu.

This article contains supporting information online at www.pnas.org/lookup/suppl/doi:10.1073/pnas.1005262107/-/DCSupplemental.

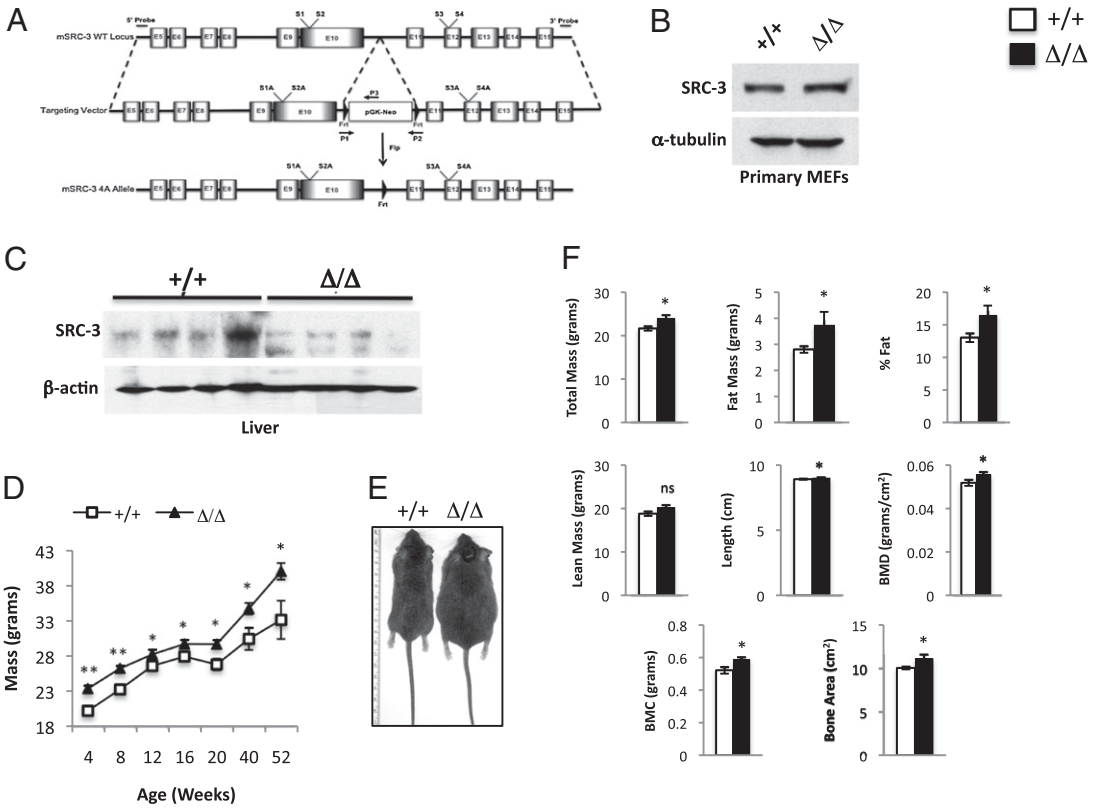

Fig. 1. Development and characterization of the SRC-3$^{\Delta/\Delta}$ mice. (*A*) Targeting construct designed to insert serine to alanine mutations into the SRC-3 gene locus. (*B*) Western blot of SRC-3 and α-tubulin from primary MEFs isolated from WT and SRC-3$^{\Delta/\Delta}$ mice. (*C*) Western blots of SRC-3 and β-actin in liver tissue isolated from WT ($n = 4$) and SRC-3$^{\Delta/\Delta}$ mice ($n = 4$). (*D*) Increased body weights in SRC-3$^{\Delta/\Delta}$ mice compared with WT littermates as observed from 4 to 52 wk. (*E*) Photograph depicts the appearance of 9-mo-old SRC-3$^{\Delta/\Delta}$ and WT littermate male mice. (*F*) DEXA body composition analysis of SRC-3$^{\Delta/\Delta}$ mice (filled bars; $n = 5$) and WT mice (open bars; $n = 5$). All data are represented as the mean ± SEM. Unpaired Student's *t* test was used to evaluate statistical significance. *, $P < 0.05$; **, $P < 0.01$.

point mutations and proper insertion of the selection cassette were used to develop chimeric mice, which were crossed to wild-type (WT) females to produce heterozygous mice (SRC-3$^{\Delta/+}$). The resulting heterozygotes were bred to generate SRC-3 homozygous knock-in mice (SRC-3$^{\Delta/\Delta}$) (Fig. S1*C*). To further confirm the presence of the engineered point mutants, RPA probes were generated to discriminate between the WT and mutant sequences (Fig. S1*D*). Point mutations in the SRC-3$^{\Delta/\Delta}$ mouse remain under the control of the endogenous promoter. qPCR revealed no changes in mRNA levels of SRC-3, or the other two SRC family members in different tissues (Fig. S1 *E–G*).

Our previous in vitro data demonstrated that mutation of certain conserved phosphorylation sites might be sufficient to alter the protein levels of SRC-3 (3). To evaluate the collective effect of the four knock-in point mutations on SRC-3 protein stability, Western blot analysis was performed on mouse embryonic fibroblasts (MEFs) isolated from WT and SRC-3$^{\Delta/\Delta}$ mice (Fig. 1*B*). These results suggest that the knock-in mutations have no significant effect on SRC-3 protein expression. Moreover, MEF cells were treated with cycloheximide for stability analyses showed a slight increase in the half-life of SRC-3 (Fig. S1*H*). Additionally, Western blot analysis of liver tissue isolated from knock-in and WT mice revealed no substantial differences in the in vivo protein expression of SRC-3 (Fig. 1*C*).

SRC-3$^{\Delta/\Delta}$ Mice Display Increased Body Weight and Composition. Initial observations of the SRC-3$^{\Delta/\Delta}$ mice revealed an increase in body weight starting just before weaning and continuing throughout life. This phenotype is opposite of what was observed in growth of SRC-3$^{-/-}$ mice (18). Body weight of the SRC-3$^{\Delta/\Delta}$ mice was initially ≈10% greater than WT, but this difference continued and became greater with age (Fig. 1*D*). At 1 y of age, SRC-3$^{\Delta/\Delta}$ mice were ≈15% larger than WT mice (Fig. 1*E*), suggesting a global growth enhancement. Body composition analysis revealed that SRC-3$^{\Delta/\Delta}$ mice have a comprehensive increase in whole body architecture (Fig. 1*F*). Interestingly, SRC-3$^{\Delta/\Delta}$ mice had more fat mass but no statistical difference in lean body mass, indicative of increased adiposity.

SRC-3$^{\Delta/\Delta}$ Mice Show Global Metabolic Defects. To better understand the cause of the increased body weight and composition in the SRC-3$^{\Delta/\Delta}$ mice, we evaluated a number of metabolic parameters. Resting energy expenditure and heat production, as measured by indirect calorimetry, revealed no differences between SRC-3$^{\Delta/\Delta}$ and WT mice (Fig. S2 and Fig. 2*A*). Upon exercise-induced stress, SRC-3$^{\Delta/\Delta}$ mice showed a minimal reduction in energy expenditure, but this difference is unlikely to explain the changes in body weight (Fig. 2*B*). Based on the persistent increase in body weight, we evaluated food intake as an assessment of metabolic homeostasis and, surprisingly, found that SRC-3$^{\Delta/\Delta}$ mice had a minor reduction in food consumption (Fig. 2*C*). Further evaluation of energy absorption, as measured by monitoring mice in metabolic cages, revealed that SRC-3$^{\Delta/\Delta}$ mice had reduced waste disposal (Fig. S3 *A–C*), most likely resulting from a decrease in food intake, but increased absorption cannot be completely excluded.

Body composition and metabolic activity have been well established to influence physical activity (19). Metabolic monitoring of locomotor activity revealed a substantial decrease in activity in SRC-3$^{\Delta/\Delta}$ mice (Fig. 2 *D–G*). Additionally, SRC-3$^{\Delta/\Delta}$ mice showed a significant reduction in resting body temperature, another index

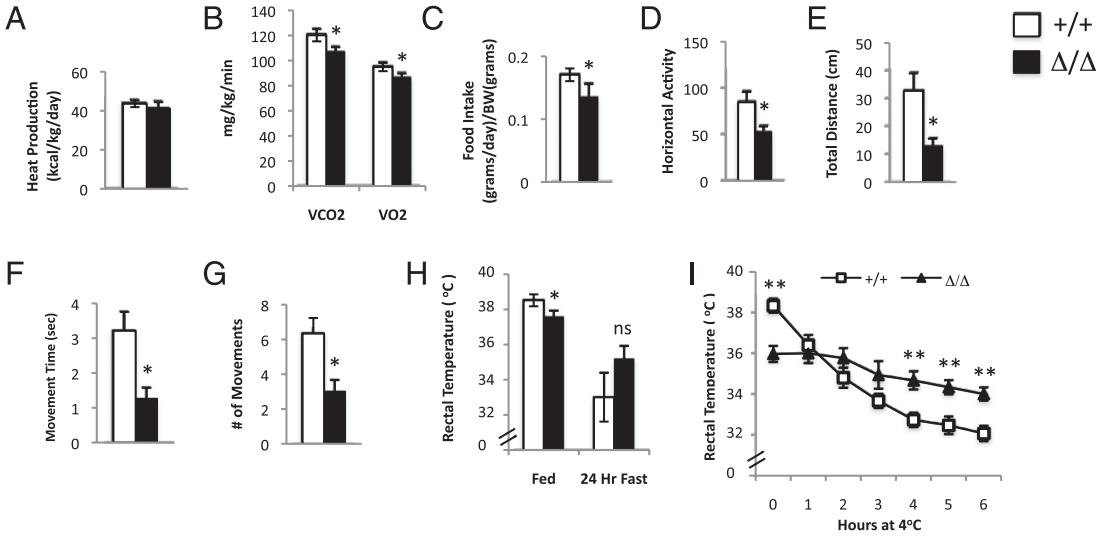

Fig. 2. SRC-3$^{\Delta/\Delta}$ mice show global metabolic defects. (*A*) Heat generation of SRC-3$^{\Delta/\Delta}$ mice (filled bars, $n = 6$) and WT (open bars, $n = 6$) littermate mice. (*B*) Exercise-induced calorimetry of SRC-3$^{\Delta/\Delta}$ (filled bars; $n = 6$) and WT mice (open bars; $n = 6$). (*C*) SRC-3$^{\Delta/\Delta}$ mice (filled bars; $n = 6$) have reduced food intake compared with WT mice (open bars; $n = 6$). (*D–G*) Locomotor activity was measured in SRC-3$^{\Delta/\Delta}$ (filled bars; $n = 6$) and WT mice (open bars; $n = 6$). The average horizontal movement, distance traveled, movement time, and number of movements during a 24-h monitoring period are shown. (*H*) Resting rectal body temperature of SRC-3$^{\Delta/\Delta}$ mice (filled bars; $n = 5$) compared with WT littermate mice (open bars; $n = 5$) during fed or 24 h fasted conditions. (*I*) Adaptive thermogenesis of SRC-3$^{\Delta/\Delta}$ mice (filled bars; $n = 6$) compared with WT littermate mice (open bars; $n = 6$) measured over a 6-h period. All data are represented as the mean ± SEM. Unpaired Student's *t* test was used to evaluate statistical significance. *, $P < 0.05$; **, $P < 0.01$.

of basal metabolic homeostasis (Fig. 2*H*). SRC-3$^{\Delta/\Delta}$ mice appear to be protected slightly from decreased body temperature in response to fasting (Fig. 2*H*). A more definitive analysis of adaptive thermogenesis clearly revealed that although SRC-3$^{\Delta/\Delta}$ mice initially showed a slightly reduced body temperature, these mice are able to maintain body temperature in response to cold (Fig. 2*I*).

SRC-3$^{\Delta/\Delta}$ Mice Exhibit Elevated IGF1 Signaling. Whole-body composition analysis of the SRC-3$^{\Delta/\Delta}$ mice suggested an increase in a global growth-controlling pathway. A previous study from our laboratory revealed that ablation of SRC-3 reduces IGF1 by decreasing SRC-3-mediated IGFBP3 gene transcription (14). Conversely, SRC-3$^{\Delta/\Delta}$ mice showed a marked increase in total plasma IGF1 (Fig. 3*A*). Analysis of IGF1 gene transcription in both liver and kidney revealed that elevated circulating levels of IGF1 were not likely due to increased synthesis of the hormone (Fig. S4*B*). Evaluation of in vivo human IGF1 turnover revealed no significant differences in the SRC-3$^{\Delta/\Delta}$ mice (Fig. S4*C*); however, this result could be partially influenced by elevated levels of mouse IGF1 in the circulation. Analysis of plasma IGFBP3 by ELISA

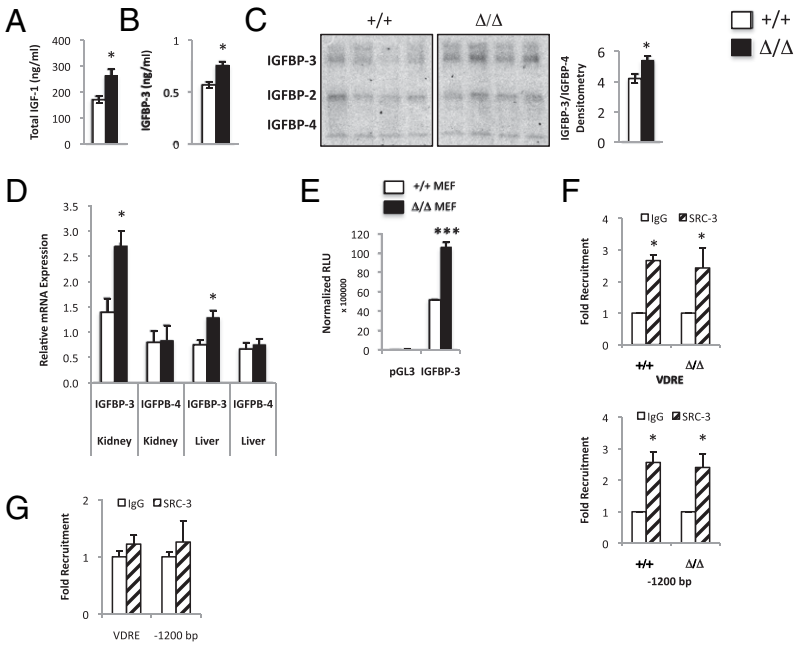

Fig. 3. SRC-3$^{\Delta/\Delta}$ mice exhibit elevated IGF1 signaling. (*A*) Plasma levels of total IGF1 in SRC-3$^{\Delta/\Delta}$ mice (filled bars; $n = 5$) compared with WT littermate mice (open bars; $n = 5$). (*B*) ELISA analysis of plasma IGFBP3 in SRC-3$^{\Delta/\Delta}$ mice ($n = 5$) compared with WT littermate mice ($n = 5$). (*C*) Analysis of plasma IGF binding proteins (IGFBP-2, -3, -4) in SRC-3$^{\Delta/\Delta}$ mice ($n = 5$) compared with WT littermate mice ($n = 5$) measured by ^{125}I-IGF1 binding. Densitometry of IGFBP3 in SRC-3$^{\Delta/\Delta}$ mice (filled bars) compared with WT littermate mice (open bars) were normalized to IGFBP4 levels. (*D*) Quantitative real-time PCR analysis of IGFBP3 and IGFBP4. RNAs were isolated from kidney and livers of SRC-3$^{\Delta/\Delta}$ (filled bars; $n = 5$) and WT littermate mice (open bars; $n = 5$). Expression levels of each gene were normalized to the levels of 18S rRNA. (*E*) SRC-3$^{\Delta/\Delta}$ mutations lead to increased transcriptional activation of the IGFBP3 promoter. Primary MEFs from SRC-3$^{\Delta/\Delta}$ (filled bars) and WT littermate mice (open bars) were transiently transfected with 3.6 Kb of the IGFBP3 WT promoter-luciferase construct or empty vector. All data were normalized to β-gal. (*F*) In vivo ChIP of SRC-3 from perfused kidney from SRC-3$^{\Delta/\Delta}$ ($n = 3$) and WT littermate mice ($n = 3$). Data are presented as fold SRC-3 signal over IgG. Amplicon is directed toward a conserved VDRE at ≈3.5 Kb or at ≈1.2 Kb upstream of the transcriptional start site, respectively. (*G*) In vivo ChIP of SRC-3 from perfused kidney from SRC-3$^{-/-}$ mice ($n = 4$). Amplicon is directed toward a conserved VDRE at ≈3.5 Kb or at ≈1.2 Kb upstream of the transcriptional start site, respectively. All data are presented as fold SRC-3 signal over IgG. All data are represented as the mean ± SEM. Unpaired Student's *t* test was used to evaluate statistical significance. *, $P < 0.05$.

revealed a moderate increase in SRC-3$^{\Delta/\Delta}$ mice (Fig. 3*B*), consistent with ligand blot analysis using ^{125}I-IGF1 to measure levels of IGF binding proteins in the circulation (Fig. 3*C*). Changes in growth hormone are known to influence the levels of IGF1, but we observed no changes in plasma growth hormone between WT and SRC-3$^{\Delta/\Delta}$ mice (Fig. S4*D*). Likewise, we observed no changes in plasma thyroid-stimulating hormone (TSH) between WT and SRC-3$^{\Delta/\Delta}$ mice (Fig. S4*E*). Synthesis of new IGF1 binding proteins primarily occurs in the kidney and, to a lesser extent, in the liver (20). Kidney and liver expression levels of IGFBP3 and IGFBP-4 mRNAs were highly consistent with IGFBP plasma levels, where SRC-3$^{\Delta/\Delta}$ mice revealed a marked increase specifically in IGFBP3 mRNA in both kidney and liver (Fig. 3*D*).

To substantiate that the effects on IGFBP3 gene transcription were mediated by mutations in SRC-3, we performed luciferase reporter assays by using a reporter construct consisting of ≈3,600 bp of the IGFBP3 proximal promoter. Consistent with the tissue expression levels of IGFBP3, primary MEFs from SRC-3$^{\Delta/\Delta}$ mice efficiently promoted gene transcription on the IGFBP3 promoter compared with WT MEFs (Fig. 3*E*). To determine whether the increased IGFBP3 gene transcription in the presence of the SRC-3 mutant is gene-specific or represents a general mechanism, we performed ERE luciferase reporter assays. Consistent with IGFBP3 gene transcription, mutant SRC-3 more efficiently coactivated ER-mediated gene transcription compared with WT SRC-3 (Fig. S4*A*), suggesting that mutant SRC-3 confers a more general increase in gene transcription. Importantly, in vivo ChIP of SRC-3 from kidney tissue isolated from SRC-3$^{\Delta/\Delta}$ and WT mice revealed no change in occupancy on the IGFBP3 promoter (Fig. 3*F*). Specificity of SRC-3 occupancy on the IGFBP3 promoter was confirmed by in vivo ChIP from kidney isolated from SRC-3$^{-/-}$ mice (Fig. 3*G*). Taken together, our data suggest that the mutations in SRC-3 confer an increase in transcriptional output of IGFBP3 independent of levels of promoter occupancy.

SRC-3$^{\Delta/\Delta}$ Mice Display the Hallmarks of Insulin Resistance. Previously reported data clearly demonstrated that overexpression of IGFBP3 in mice results in hyperglycemia and leads to reduced insulin sensitivity (21, 22). Consistent with those reports, SRC-3$^{\Delta/\Delta}$ mice developed hyperglycemia, which is observed during both ad libitum and 24-h fasting conditions (Fig. 4*A Left*). SRC-3$^{\Delta/\Delta}$ mice also displayed an elevation in fasting insulin levels (Fig. 4*A Right*), along with a decrease in fasting glucagon (Fig. S5*A*), implicating insulin resistance. The hyperglycemia appears to be age-dependent, because at a younger age, SRC-3$^{\Delta/\Delta}$ mice showed a trend toward hyperglycemia, but these data failed to reach significance (Fig. S5*B*). Moreover, a glucose tolerance test revealed that SRC-3$^{\Delta/\Delta}$ mice have abnormal glucose tolerance when compared with WT mice (Fig. 4*B Left*). In fact, even though SRC-3$^{\Delta/\Delta}$ mice showed increased circulating insulin levels in response to a glucose challenge, this adaptive response was still incapable of normalizing blood glucose (Fig. 4*B Right*). Further evaluation using an insulin tolerance test revealed that SRC-3$^{\Delta/\Delta}$ mice are less effective at achieving normoglycemia (Fig. 4*C*). Collectively, these data clearly point to the development of insulin resistance in the SRC-3$^{\Delta/\Delta}$ mouse.

Consistent with reports of the IGFBP3 transgenic mice, SRC-3$^{\Delta/\Delta}$ mice also showed increased glycogen content in liver as determined by Periodic acid-Schiff staining (PAS) (Fig. 4*D*) and enzymatic quantitation (Fig. 4*E*). In line with insulin resistance, SRC-3$^{\Delta/\Delta}$ mice showed increased hepatic storage of triglycerides (Fig. 4*D*) and elevated circulating triglycerides (Fig. 4*F*). However, SRC-3$^{\Delta/\Delta}$ mice maintained normal circulating levels of cholesterol and fatty acids (Fig. S6 *A* and *B*). Also, mirroring the IGFBP3 transgenic mice, SRC-3$^{\Delta/\Delta}$ mice showed increased adiposity. This observation correlates with increased adipocyte size (Fig. 4*D*), as confirmed by quantitation of H&E sections of white adipose tissue (Fig. S6*C*), and an increase in the adipose-secreted hormone leptin (Fig. S6*D*), whereas the level of adiponectin was substantially reduced (Fig. 4*G*). Both of these adipokines serve as excellent indicators of whole body physiology. In each case, the levels of these hormones are consistent with increased insulin resistance, adiposity, and a propensity toward an obese phenotype. Unexpectedly, we found reduced adipocyte differentiation potential in MEFs

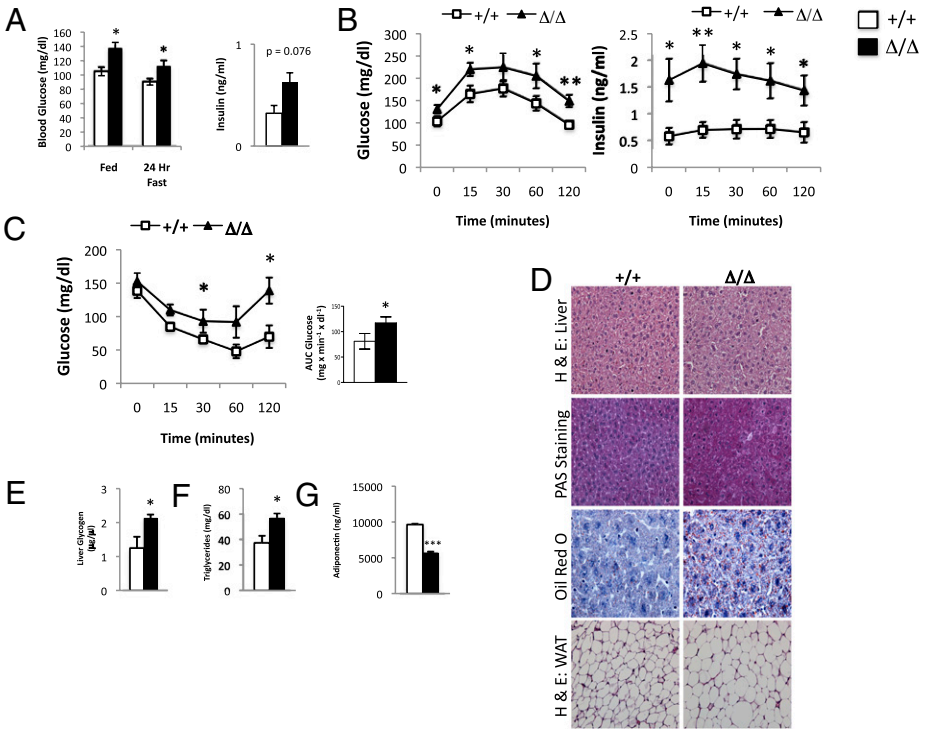

Fig. 4. SRC-3$^{\Delta/\Delta}$ mice display the hallmarks of insulin resistance. (*A*) Measurement of blood glucose and insulin levels in 9-mo-old SRC-3$^{\Delta/\Delta}$ (filled bars; n = 5) compared with WT littermate mice (open bars; n = 5) under fed or 24-h fasting conditions. (*B*) Glucose tolerance test and parallel insulin measurement of SRC-3$^{\Delta/\Delta}$ (black line, n = 6) and WT littermate mice (white line, n = 6). (*C*) Insulin tolerance test of SRC-3$^{\Delta/\Delta}$ (black line, n = 6) and WT littermate mice (white line, n = 6). Two-way ANOVA analysis performed by using Area Under the Curve (AUC) calculation of insulin tolerance test results in SRC-3$^{\Delta/\Delta}$ (filled bars; n = 6) and WT littermate mice (open bars; n = 6). (*D*) Histological examination liver sections from WT and SRC-3$^{\Delta/\Delta}$ littermate mice for H&E, Periodic acid-Schiff staining (PAS), Oil Red O, and H&E for WAT. (*E*) Quantitative enzymatic analysis of liver glycogen levels in SRC-3$^{\Delta/\Delta}$ (filled bars; n = 5) and WT littermate mice (open bars; n = 5). (*F* and *G*) Plasma profiling after 24 h fasting of triglycerides and adiponectin in SRC-3$^{\Delta/\Delta}$ (filled bars; n = 5) and WT littermate mice (open bars; n = 5). All data are represented as the mean ± SEM. Unpaired Student's t test was used to evaluate statistical significance. *, $P < 0.05$; **, $P < 0.01$.

isolated from SRC-3$^{\Delta/\Delta}$ mice compared with WT MEFs (Fig. S6*E*). qPCR analysis of adipogenic PPARγ target genes over the course of differentiation in SRC-3$^{\Delta/\Delta}$ and WT MEFs revealed no significant differences (Fig. S6*F*). Collectively, these data are consistent with impaired peripheral insulin sensitivity, hyperglycemia, and increased adiposity.

SRC-3$^{\Delta/\Delta}$ Mice Are Inherently More Susceptible to Carcinogen-Induced Tumorigenesis. The observation that SRC-3$^{\Delta/\Delta}$ mice had elevated circulating levels of IGF1 prompted us to investigate the potential consequences of this phenotype on tumorigenesis. Evaluation of total IGF1 levels in tissues of WT and SRC-3$^{\Delta/\Delta}$ mice revealed no increase in IGF1 in the liver (Fig. S7), suggesting that the elevated circulating IGF1 was primarily due to increased production of IGFBP3. To investigate the effect of elevated IGF1 in the liver, WT and SRC-3$^{\Delta/\Delta}$ mice were injected with the liver-specific carcinogen, diethylnitrosamine (DEN). After 1 y, the livers of SRC-3$^{\Delta/\Delta}$ mice appeared to be more susceptible to carcinogen-induced tumorigenesis than WT mice (Fig. 5*A*). Closer examination revealed no change in liver weight when normalized to body weight (Fig. 5*B*). SRC-3$^{\Delta/\Delta}$ mice displayed increases in the numbers of visible tumors, average tumor size, and maximal tumor size (Fig. 5 *C*–*E*). This increased tumor progression, coupled with elevated IGF1 and hyperinsulinemia in the SRC-3$^{\Delta/\Delta}$ mice, suggest that the canonical signal transduction pathways downstream of insulin and IGF1 may be elevated in these mice. Western blot analyses of liver tumor extracts revealed a clear activation of downstream components of the insulin/IGF1 signaling pathways in SRC-3$^{\Delta/\Delta}$ mice (Fig. 5*F*). Collectively, these data suggest that SRC-3 regulation of IGFBP3 influences the activation of IGF1 signaling pathways, which culminate to increase growth capacity of hepatic tumors.

Discussion

From a mechanistic perspective, SRC-3 has served as a model coactivator for how the PTM code of a "master growth coregulator" influences its cellular function. Our laboratory initially identified the mechanism by which phosphorylation of SRC-3 directly controls its transcriptional coactivation potential (4). This finding led us to discover that site-specific phosphorylation of SRC-3 also can serve as a primer for subsequent ubiquitylation, which can be a prerequisite for maximal transcriptional activity and temporal turnover of SRC-3 (3). In addition to these studies, we have demonstrated how phosphorylation of SRC-3 by different kinases, and at different residues, confers distinct genetic consequences. Although these data collectively point to the importance of the PTM code in modulating the diverse functions of SRC-3, understanding how this PTM code manifests changes at the physiological level had not been evaluated. Thus, the development of the SRC-3$^{\Delta/\Delta}$ mouse provided a unique and necessary tool to test the in vivo significance of changes in the PTM code on SRC-3 systemic function.

The widespread metabolic changes observed in our PTM knock-in model, coupled with impaired glucose homeostasis and increased body weight, suggest that in vitro approaches are effective for evaluating specific gene functions (and pathways) of phosphorylation sites, but often are incomplete in terms of predicting systemic physiological consequences. The metabolic alterations observed in the present study suggest that the four specific knock-in mutations converge on a global growth-signaling pathway in a way that could not be predicted in advance. We reported that deletion of the SRC-3 gene negatively impacts IGF1 signaling in mice, likely resulting from impaired transcription of the IGFBP3 gene (14). This deficiency reduces the pool of circulating IGF1 and contributes to the decreased body weight observed in the SRC-3$^{-/-}$ mice. Conversely, analysis of SRC-3$^{\Delta/\Delta}$ mice revealed a marked increase in plasma IGF1 levels, which correlates with (or likely results from) markedly elevated transcript and protein levels of IGFBP3. One functional outcome of this elevated IGF1 signaling is enhanced susceptibility to carcinogen-induced tumor growth. Although, we are unable to definitively discriminate between the direct oncogenic functions of mutant SRC-3 and the role that these mutations play in bolstering IGF1 signaling, it is reasonable to assume that even indirectly, PTMs

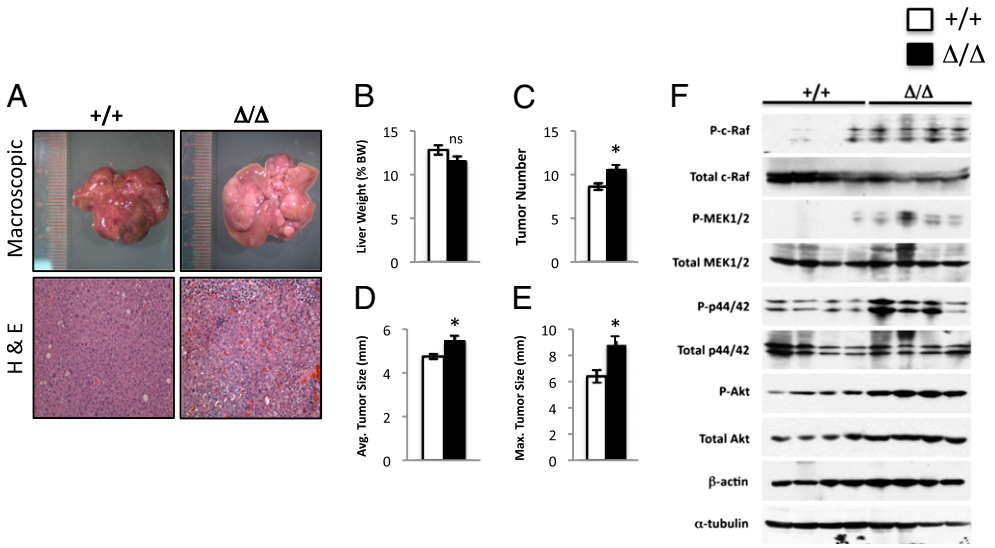

Fig. 5. SRC-3$^{\Delta/\Delta}$ mice are inherently more susceptible to carcinogen-induced tumorigenesis. (*A*) Representative macroscopic analysis of livers isolated from SRC-3$^{\Delta/\Delta}$ and WT littermate male mice treated for 12 mo with DEN (*Upper*). H&E staining of formalin-fixed livers from DEN-treated SRC-3$^{\Delta/\Delta}$ and WT mice (*Lower*). (*B*) Measurement of liver weight as a percentage of body weight in DEN-treated SRC-3$^{\Delta/\Delta}$ (filled bars; $n = 5$) and WT littermate mice (open bars; $n = 5$). (*C*) Analysis of total tumor number from DEN-treated SRC-3$^{\Delta/\Delta}$ (filled bars; $n = 5$) and WT littermate mice (open bars; $n = 5$). (*D*) Measurement of average tumor size determined in *C* in DEN-treated SRC-3$^{\Delta/\Delta}$ (filled bars; $n = 5$) and WT littermate mice (open bars; $n = 5$). (*E*) Measurement of maximal tumor size determined from *C* in DEN-treated SRC-3$^{\Delta/\Delta}$ (filled bars; $n = 5$) and WT littermate mice (open bars; $n = 5$). (*F*) Western blots of phosphorylated and total c-Raf, MEK1/2, p44/42, Akt, as well as α-tubulin and β-actin from liver tumor tissue isolated from WT ($n = 4$) and SRC-3$^{\Delta/\Delta}$ littermate mice ($n = 4$). All data are represented as the mean ± SEM. Unpaired Student's *t* test was used to evaluate statistical significance. *, $P < 0.05$.

on SRC-3 produce secondary effects on tumor growth, in addition to its more direct oncogenic potential when overexpressed.

Several groups have reported on transgenic mouse models overexpressing IGFBP3 (21, 22), which phenotypically share a number of similarities to the SRC-$3^{\Delta/\Delta}$ mice. In particular, overexpression of IGFBP3 results in elevated circulating levels of IGF1, insulin resistance, and hyperglycemia, all of which were observed in our SRC-$3^{\Delta/\Delta}$ mouse model. Additionally, both SRC-$3^{\Delta/\Delta}$ and IGFBP3 transgenic mice show a marked increase in epididymal fat pad mass. Surprisingly, in the SRC-$3^{\Delta/\Delta}$ mice, this increase is not due to enhanced adipocyte differentiation, but rather when coupled with elevated levels of triglycerides in the liver and the circulation, likely points to increased lipogenesis. Again, these observations are consistent with increased IGF1 signaling.

The obese phenotype observed in our SRC-$3^{\Delta/\Delta}$ mice was accompanied by the development of age-dependent insulin resistance and hyperglycemia. Accordingly, the phenotype of our mouse model resembles the metabolic syndrome seen in humans. This observation raises the interesting question whether PTM modifications of SRC-3 (or other coactivators) could play a role in the development of obesity and type 2 diabetes. Because an increased prevalence of some types of cancer occurs in concert with obesity, another interesting question is whether SRC-3 could serve as a link between these two conditions. Collectively, our work provides evidence that functional combinations of endogenous PTMs can reprogram a single coactivator like SRC-3 for specific functions that completely alter the systems biology of an organism. Especially compared with the growth and metabolic phenotypes of the SRC-$3^{-/-}$ mice, our SRC-$3^{\Delta/\Delta}$ mice emphasize the general importance of PTMs as they relate to in vivo coregulator function. Perhaps such studies of coregulator PTMs will provide new therapeutic insights for intervention in diseases such as type 2 diabetes, obesity, and cancer.

Experimental Procedures

Generation of SRC-$3^{\Delta/\Delta}$ Mice. Complete details for generation of SRC-$3^{\Delta/\Delta}$ mice is described in the *SI Experimental Procedures*.

qPCR Assays. Total mRNA was isolated from liver, muscle, brain, WAT, or kidney by using the RNeasy Kit (Qiagen). Reverse transcription was carried out by using the SuperScript II kit (Invitrogen) per the manufacturer's instructions. For gene expression analysis, qPCR was performed by using sequence-specific primers and the Universal Probe Library (Roche). For all analyses, 18S was used as an internal control. Sequences of all qPCR primers are available upon request.

Cell Culture, Transient Transfection, and Luciferase Assays. Primary WT and SRC-$3^{\Delta/\Delta}$ MEFs were maintained in DMEM with 10% FBS. For transient-transfection assays, MEFs were plated in six-well plates overnight and transfected with pGL3-basic or pGL3-IGFBP3 (1-3590) plasmid containing the luciferase reporter by using the FuGENE 6 HD transfection reagent (Roche). All cells were cotransfected with the pRSV-β-gal expression plasmid as a control for transfection efficiency. Cell lysates were prepared 48 h after transfection, and the β-gal and luciferase activities were measured with a luciferase assay kit (Promega). The relative luciferase units were normalized to the β-gal activity.

Chromatin Immunoprecipitation. In vivo kidney ChIP was performed as described (http://genomics.ucdavis.edu/farnham/protocols/tissues.html). Briefly, ≈100 mg of whole kidney tissue isolated from SRC-$3^{\Delta/\Delta}$, SRC-$3^{+/+}$, or SRC-$3^{-/-}$ mice was finely minced, cross-linked with 1% methanol-free formaldehyde for 15 min, quenched in 125 mM glycine, and centrifuged at 2,000 × *g* at 4 °C. The resulting pellets were Dounce homogenized in PBS containing Mg^{2+}/Ca^{2+}, protease inhibitors, and phosphatase inhibitors, then centrifuged again. Pellets were resuspended in 300 μL of sonication buffer, and 100 μL of sonicated chromatin was immunoprecipitated with 4 μg of SRC-3 antibody (sc-7216) or normal IgG (sc-2028) per our standard protocol. All primer sequences are available upon request.

Tumor Induction and Analysis. Fifteen-day-old pups (SRC-$3^{\Delta/\Delta}$ and WT littermates) were IP injected with 10 mg/kg diethylnitrosamine (Sigma). After 12 mo on normal chow, mice were weighed, killed, and their livers were removed, analyzed, and photographed macroscopically. Livers were further evaluated to determine the total tumor number, average tumor size, maximal tumor size, and liver weight. Samples of each liver tissue were prepared for histology as described (23).

Statistical Analyses. All results are shown as the mean ± SEM. The comparison of different groups was carried out by using two-tailed unpaired Student's *t* test, and differences at or below $P < 0.05$ were considered statistically significant.

ACKNOWLEDGMENTS. We thank Suoling Zhou, Lan Liao, and Alison Belcher for technical assistance and A. F. Parlow at the National Institute of Diabetes and Digestive and Kidney Diseases (NIDDK) National Hormone & Peptide Program. J.V.S. is funded by the Norwegian Cancer Society, University of Bergen, Det regionale samarbeidsorganet (Helse Vest RHF and University of Bergen), and the Norwegian Society of Endocrinology. This work was partially supported by NIH Grants R01 DK058242 and R01 CA112403 (to J. Xu), Susan G. Komen Grant BCTR0707225 (to R.C.W.), and National Institutes of Health (NIH)-DDC Core Morphology Lab Grant DK56338. Nuclear Receptor Signaling Atlas/NIDDK U19 DK62434-08 and NIDDK P01 HD8818-37 (to B.W.O.) provided the primary support for this work.

1. Chauchereau A, Amazit L, Quesne M, Guiochon-Mantel A, Milgrom E (2003) Sumoylation of the progesterone receptor and of the steroid receptor coactivator SRC-1. *J Biol Chem* 278:12335–12343.
2. Hoang T, et al. (2004) cAMP-dependent protein kinase regulates ubiquitin-proteasome-mediated degradation and subcellular localization of the nuclear receptor coactivator GRIP1. *J Biol Chem* 279:49120–49130.
3. Wu RC, Feng Q, Lonard DM, O'Malley BW (2007) SRC-3 coactivator functional lifetime is regulated by a phospho-dependent ubiquitin time clock. *Cell* 129:1125–1140.
4. Wu RC, et al. (2004) Selective phosphorylations of the SRC-3/AIB1 coactivator integrate genomic reponses to multiple cellular signaling pathways. *Mol Cell* 15:937–949.
5. Lonard DM, Lanz RB, O'Malley BW (2007) Nuclear receptor coregulators and human disease. *Endocr Rev* 28:575–587.
6. Picard F, et al. (2002) SRC-1 and TIF2 control energy balance between white and brown adipose tissues. *Cell* 111:931–941.
7. Chopra AR, et al. (2008) Absence of the SRC-2 coactivator results in a glycogenopathy resembling Von Gierke's disease. *Science* 322:1395–1399.
8. Louet JF, et al. (2006) Oncogenic steroid receptor coactivator-3 is a key regulator of the white adipogenic program. *Proc Natl Acad Sci USA* 103:17868–17873.
9. Coste A, et al. (2008) The genetic ablation of SRC-3 protects against obesity and improves insulin sensitivity by reducing the acetylation of PGC-1alpha. *Proc Natl Acad Sci USA* 105:17187–17192.
10. Lonard DM, O'Malley BW (2007) Nuclear receptor coregulators: Judges, juries, and executioners of cellular regulation. *Mol Cell* 27:691–700.
11. Louie MC, Zou JX, Rabinovich A, Chen HW (2004) ACTR/AIB1 functions as an E2F1 coactivator to promote breast cancer cell proliferation and antiestrogen resistance. *Mol Cell Biol* 24:5157–5171.
12. Fereshteh MP, et al. (2008) The nuclear receptor coactivator amplified in breast cancer-1 is required for Neu (ErbB2/HER2) activation, signaling, and mammary tumorigenesis in mice. *Cancer Res* 68:3697–3706.
13. Gao Z, et al. (2005) Coactivators and corepressors of NF-kappaB in IkappaB alpha gene promoter. *J Biol Chem* 280:21091–21098.
14. Liao L, Chen X, Wang S, Parlow AF, Xu J (2008) Steroid receptor coactivator 3 maintains circulating insulin-like growth factor I (IGF-I) by controlling IGF-binding protein 3 expression. *Mol Cell Biol* 28:2460–2469.
15. Yan J, et al. (2006) Steroid receptor coactivator-3 and activator protein-1 coordinately regulate the transcription of components of the insulin-like growth factor/AKT signaling pathway. *Cancer Res* 66:11039–11046.
16. Kuang SQ, et al. (2004) AIB1/SRC-3 deficiency affects insulin-like growth factor I signaling pathway and suppresses v-Ha-ras-induced breast cancer initiation and progression in mice. *Cancer Res* 64:1875–1885.
17. Xu J, Wu RC, O'Malley BW (2009) Normal and cancer-related functions of the p160 steroid receptor co-activator (SRC) family. *Nat Rev Cancer* 9:615–630.
18. Xu J, et al. (2000) The steroid receptor coactivator SRC-3 (p/CIP/RAC3/AIB1/ACTR/TRAM-1) is required for normal growth, puberty, female reproductive function, and mammary gland development. *Proc Natl Acad Sci USA* 97:6379–6384.
19. Ekelund U, Franks PW, Sharp S, Brage S, Wareham NJ (2007) Increase in physical activity energy expenditure is associated with reduced metabolic risk independent of change in fatness and fitness. *Diabetes Care* 30:2101–2106.
20. Lemmey AB, Glassford J, Flick-Smith HC, Holly JMP, Pell JM (1997) Differential regulation of tissue insulin-like growth factor-binding protein (IGFBP)-3, IGF-I and IGF type 1 receptor mRNA levels, and serum IGF-I and IGFBP concentrations by growth hormone and IGF-I. *J Endocrinol* 154:319–328.
21. Modric T, et al. (2001) Phenotypic manifestations of insulin-like growth factor-binding protein-3 overexpression in transgenic mice. *Endocrinology* 142:1958–1967.
22. Silha JV, Gui Y, Murphy LJ (2002) Impaired glucose homeostasis in insulin-like growth factor-binding protein-3-transgenic mice. *Am J Physiol Endocrinol Metab* 283: E937–E945.
23. Wang L, et al. (2005) The orphan nuclear receptor SHP regulates PGC-1alpha expression and energy production in brown adipocytes. *Cell Metab* 2:227–238.